Natural Resources for Human Health
eISSN: 2583-1194

Original Research

Received 29 July 2026
Revised 23 Aug 2026
Accepted 07 Sep 2026

Natural Resources for Human Health 2026, Vol. 6 (21s): 725–746

KEYWORDS:
Urban heat Island; UHI mitigation; Reflective Pavement; Rigid Pavement Concrete; Supplementary Cementitious Materials; Recycled Plastic Aggregate; Taguchi Optimization

Thermo-Mechanical Performance of Macro-Polymer Modified Sustainable Rigid Pavement Concrete for Urban Heat Island Mitigation

Lovneesh Sharma[1]*, Shristi Kanoungo[1], Abhishek Kanoungo[2]

[1]Chitkara University Institute of Engineering and Technology, Chitkara University, Punjab, India
[2]Chitkara University School of Engineering & Technology, Chitkara University, Himachal Pradesh, India.
*Corresponding Author: Lovneesh Sharma
Email Id- lovneeshsharma39@gmail.com

ABSTRACT: The urban heat island effect, driven largely by heat absorption and retention by paved surfaces, remains a major challenge in sustainable urban development. This study presents a systematic three-stage experimental program to assess supplementary materials in rigid pavement concrete for improving mechanical performance and reducing surface temperature. Stage I examined single-material replacements of 5–35%, including natural zeolite and hydrated lime as partial Ordinary Portland Cement replacements, steel slag as fine aggregate replacement, and recycled plastic aggregate (RPA) as coarse aggregate replacement. Stage II identified optimum levels of cementitious modifiers and RPA, while Stage III evaluated triple-modified mixes with simultaneous cementitious, fine aggregate, and coarse aggregate substitutions. The surface temperature of the specimens was measured using infrared thermometry. The Jonckheere–Terpstra test confirmed statistically significant trends for zeolite, steel slag, and RPA replacements ($p \leq 0.042$). Stage I optimum levels were 15% zeolite, 10% lime, and 20% steel slag, yielding compressive strength improvements of 10.9%, 4.5%, and 12.5%, respectively, over the control, whereas RPA caused progressive strength reduction. The optimum triple-modified mix, Z15R5S20, achieved a 28-day compressive strength of 50.5 MPa, a 14.8% increase over the control, and a 7.5 °C surface temperature reduction. Taguchi S/N analysis confirmed this optimum mix with a prediction error of 0.62%. A strong negative Pearson correlation between compressive strength and surface temperature ($r = -0.83$, $p < 0.001$) demonstrated the potential to balance structural performance and thermal mitigation. The findings indicate a technically viable and environmentally sustainable approach for UHI mitigation in urban pavements.

1. INTRODUCTION

Rapid urban development has substantially altered the thermal behaviour of urban centres, leading to the Urban Heat Island (UHI) effect, characterized by higher surface and ambient temperatures in urban areas than in surrounding rural regions [1,2]. UHI is associated with increased cooling energy demand, which may reach 20–30% in some high-temperature cities [3,4], elevated Ground Level Ozone (GL-O_2) concentrations, reduced thermal comfort, and increased heat-related morbidity. Pavement systems are among the major contributors to anthropogenic heat accumulation from horizontal urban surfaces, including roads, parking lots, walkways, and commercial and residential developments, accounting for nearly 30–40% of heat absorption in dense urban cores [5,6]. Conventional pavement materials, mainly dense bitumen and cement-based concrete, are dark in colour, have limited evaporative cooling potential, low albedo, and high thermal storage capacity, thereby intensifying UHI effects.

Portland Cement Concrete (PCC), commonly used in rigid pavements, has high thermal mass and relatively low surface albedo, approximately 0.25–0.35 for aged concrete [7]. It absorbs substantial short-wave solar radiation during the day and releases

stored heat as long-wave radiation at night, contributing to elevated nighttime temperatures, a key feature of UHI. Existing pavement-based UHI mitigation strategies broadly include reflective or "cool" pavements, permeable pavements, phase-change material (PCM)-incorporated pavements, and material-composition modifications that alter the thermophysical properties of concrete [2,3,8]. Qin et al. [3] reported that reflective coatings can reduce pavement surface temperature by 4–10 °C during peak insolation. However, traffic-induced wear, abrasion, and soiling can significantly reduce albedo within 2–3 years of service, limiting long-term effectiveness [9]. Similarly observed that albedo values of freshly placed white cement concrete ranged from 0.45 to 0.60 but decreased to 0.30–0.40 due to ageing and soiling [10, 11].

These limitations have shifted research attention toward intrinsic modification of the concrete matrix as a more durable and structurally viable UHI mitigation approach. Mohajerani et al. [7] established relationships among surface albedo, thermal conductivity, and nocturnal heat flux, and highlighted that aggregate-phase thermal conductivity strongly influences subsurface heat storage. This suggests that replacing conventional aggregates with thermally modified or low-conductivity alternatives may help limit heat accumulation within pavement systems. Given the long service life of rigid pavements, typically 30–50 years, material-level interventions offer a durable means of reducing UHI impacts while maintaining structural performance.

In parallel, increasing environmental concerns have placed pressure on the construction sector to reduce carbon emissions and dependence on natural resources. Cement production alone contributes approximately 7–8% of total anthropogenic CO_2 emissions [12], while natural aggregate extraction causes ecological disruption. Supplementary cementitious materials (SCMs), such as zeolite, lime, and fly ash, offer dual benefits by reducing clinker dependence and modifying concrete microstructure to improve durability and, potentially, thermal performance.

Natural zeolites, particularly clinoptilolite-rich aluminosilicates, are microporous crystalline materials composed of three-dimensional SiO_4 and AlO_4 tetrahedral frameworks. They have gained attention as SCMs due to their pozzolanic reactivity, ion-exchange capacity, and natural availability [13-15]. Ahmadi and Shekarchi [13] reported that 10–15% replacement of Ordinary Portland Cement (OPC) with clinoptilolite-rich zeolite produced optimum performance, with 8–12% higher 28-day compressive strength than the control mix. Reactive SiO_2 and Al_2O_3 in zeolite consume $Ca(OH)_2$ during hydration, forming secondary calcium silicate hydrate (C-S-H) gel, refining the pore structure, and strengthening the interfacial transition zone (ITZ). Authors further reported that 15% zeolite reduced water absorption and chloride permeability while maintaining compressive strength within 5% of the control [16]. Zeolite's internal porosity may also support water absorption, internal curing, and evaporative cooling under thermal loading, although this effect remains insufficiently quantified in pavement applications [13].

Hydrated lime, $Ca(OH)_2$, has long been used as a stabiliser and supplementary binder in construction materials. In cement-based systems, it modifies hydration kinetics by supplying additional portlandite, which can participate in secondary pozzolanic reactions within the ITZ [17]. Arandigoyen and Alvarez reported that cement-lime mortars with 5–15% lime showed a 3–8% compressive strength improvement at low replacement levels, while higher dosages increased the effective water-to-cement ratio and caused significant strength loss. Thus, lime is more effective as a microstructural modifier than as a primary strength-contributing material, particularly when combined with reactive pozzolanic materials capable of consuming supplementary $Ca(OH)_2$.

Steel slag, a by-product of steelmaking, has been widely investigated as a natural fine aggregate substitute in pavement concrete due to its hardness, angularity, abrasion resistance, and latent hydraulic properties [18,19]. Researchers reported that Electric Arc Furnace (EAF) steel slag concrete achieved 15–25% higher compressive strength than conventional concrete due to rough surface texture, angular morphology, and improved aggregate-paste bonding [19]. Manso and co-workers showed that pre-aged EAF slag, stored outdoors for at least three months, effectively controlled expansion cracking caused by free CaO and MgO hydration. Compressive strength exceeded control values up to 25% slag replacement but declined at 30–35% due to volumetric instability[18]. Thermally, steel slag may offer higher visible-spectrum reflectance than darker conventional aggregates due to its lighter colour and glassy surface phase [7,14,20].

Recycled plastic aggregate (RPA) has also emerged as a potential substitute for natural coarse aggregate, addressing the growing problem of plastic waste management. Authors reviewed more than 80 studies and identified two major limitations of recycled plastic in concrete: hydrophobic and smooth plastic surfaces weaken ITZ bonding, while lower stiffness and strength reduce concrete load-bearing capacity [21]. Reported compressive strength reductions ranged from 5–10% at 5% replacement to 40–45% at 30–35% replacement, consistent with the present investigation. Some studies confirmed that strength reduction is

generally unavoidable unless corrective measures are applied [22-24]. However, plastic aggregate has low thermal conductivity, approximately 0.15–0.24 W/m·K compared with 1.5–2.5 W/m·K for mineral aggregates, which can reduce heat transmission through pavement slabs. The researchers further noted that RPA-induced macro-voids and porosity create air-filled insulating regions. While this improves bulk thermal resistance, large surface voids may trap heat and increase surface temperature, requiring direct thermal evaluation [25].

Although SCMs and alternative aggregates have been studied individually, limited large-scale research has incorporated multiple complementary materials into a single concrete matrix and systematically correlated mechanical and thermal behaviour. Most existing studies focus on either mechanical performance or environmental sustainability, with comparatively limited attention to UHI mitigation [26, 27]. However, rigid pavement suitability cannot be assessed on thermal performance alone. Critical parameters such as compressive strength, flexural and tensile strength, fatigue resistance, and long-term durability under aggressive urban service conditions must also be satisfied [28]. Fly ash can partially compensate for strength loss caused by rubber aggregates, demonstrating the feasibility of compensatory multi-material systems. However, no documented study has combined pozzolanic cementitious modifiers, recycled plastic aggregates, and industrial slags within a single three-stage framework with simultaneous mechanical and thermal performance evaluation [29].

From a methodological perspective, the Taguchi design-of-experiments (DOE) approach has been applied in limited concrete mix optimisation studies. Its quality engineering foundation was established by Ross [30], while signal-to-noise (S/N) ratio analysis has been used to optimise SCM-modified concrete for compressive strength, durability, and workability [31]. However, its application to simultaneous mechanical and thermal optimisation of pavement concrete remains unreported. provides the analytical framework for interpreting ANOVA on S/N ratios and applying the additive model for confirmation testing, which is adopted in this study [32].

Therefore, the primary aim of this study is to reduce UHI effects through the use of SCMs and alternative aggregates in M40 rigid pavement concrete. The specific objectives are: (i) to design and evaluate concrete mixes containing zeolite, lime, RPA, and steel slag through a three-stage process of increasing material complexity; (ii) to compare compressive, split tensile, and flexural strength at five curing ages with statistical validation; (iii) to assess the thermal behaviour of Stage III mixes under simulated solar radiation using infrared thermometry; and (iv) to apply the Taguchi DOE methodology to determine the optimum mix and quantify the contribution of each factor. Finally, a trade-off between mechanical and thermal improvements is established to define concurrent optimality. The findings are expected to provide a financially viable and environmentally sustainable approach for utilizing industrial waste in rigid pavement systems while contributing to UHI mitigation, metropolitan infrastructure resilience, sustainable urban development, and circular economy practices.

2. MATERIALS AND EXPERIMENTAL METHODOLOGY

2.1 Experimental Design and Research Framework

The experimental programme was designed into three progressive stages. Four single material replacements at seven different mixing percentages (5%, 10% increments up to 35%) were tested in Stage I: (a) natural zeolite provided as partial replacement to OPC; (b) hydrated lime provided as partial replacement to OPC; (c) steel slag provided as partial fine aggregate; (d) RPA provided as partial coarse aggregate replacement (**Fig. 1**). This resulted in 28 modified mixes and one control (C-0) which added up to 29 Stage I mixes. In Stage II, the best cementitious modifier from Stage I was used with 5–35% RPA, resulting in 10 mixes in two series: zeolite–RPA and lime–RPA. Stage III explored the optimum cementitious modifier combined with RPA at both 5% and 10% and with steel slag ranging from 10% to 25%, resulting in a full 2 × 2 × 4 factorial design experimental matrix with 16 experimental mixes, which also represented the mix design for the Taguchi Design-of-Experiments (DOE) analysis.

2.2 Materials

2.2.1 Ordinary Portland Cement (OPC)

OPC of 43 grade conforming to IS 8112:2013 [33] is used as the primary binder as shown in **Fig. 1.** The specific gravity of cement is 3.15, the initial setting time as 32 minutes, the final setting time as 285 minutes, the Blaine specific surface area as 3100 cm^2/g, and the 28-day compressive strength of cement (Standard mortar) was 48.2 MPa. The chemical composition comprises of CaO (63.5%), SiO_2 (21.2%), Al_2O_3 (5.4%), Fe_2O_3 (3.8%), MgO (1.5%), SO_3 (2.3%), and loss on ignition (1.8%).

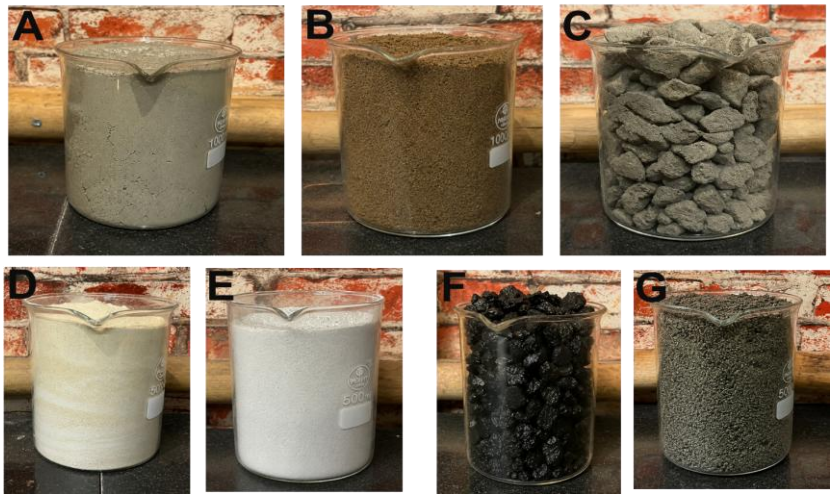


Fig. 1. Material used in preparation of Concrete, A) Cement, B) Fine Aggregate C) Coarse Aggregate, D) Natural Zeolite, E) Hydrated Lime, F) Recycled Plastic Aggregate, G) Steel Slag.

2.2.2 Fine Aggregate (Natural River Sand)

Natural river sand conforming to Zone II grading as per IS 383:2016 [34] is used as fine aggregate as shown in **Fig. 1**. Specific gravity of sand is 2.65, fineness modulus is 2.78, bulk density is 1620 kg/m³ and water absorption is 1.2%. The particle size distribution checked within Zone II limits: (100 % passed the 4.5 mm sieve and 2 % retained on the 2.36 mm sieve). The sand was free from organic impurities as verified by the colour test (IS 2386 Part II).

2.2.3 Coarse Aggregate

Crushed granite aggregate with a nominal maximum size of 20 mm and conforming to IS 383:2016 is used as coarse aggregate in the control mix as shown in **Fig. 1**. The specific gravity of the aggregate is 2.72, water absorption is 0.6%, bulk density is 1480 kg/m³, Los Angeles abrasion value is 22% and aggregate impact value is 18%. Grading for 20 mm and 10 mm fraction (60:40 ratio) was found to be in accordance to Table 2 of IS 383:2016.

2.2.4 Natural Zeolite

The natural clinoptilolite contaminated zeolite has been obtained and ground to the cement like fineness (corresponding to a Blaine specific surface area of 3200 cm²/g with a median particle diameter D50 of 22 μm) in a ball mill as shown in **Fig. 1**. The zeolite had a specific gravity of 2.20. Chemical characterisation by XRF analysis revealed: SiO_2 (67.3%), Al_2O_3 (12.8%), CaO (3.1%), Fe_2O_3 (1.4%), K_2O (2.9%), Na_2O (1.1%), MgO (0.8%), and loss on ignition (7.2%). The high level of SiO_2 + Al_2O_3 (80.1%) meets the pozzolanic requirement designated in ASTM C618 [45]. Zeolite has been chosen because of its potential pozzolanic reactivity which offers the advantages to increase the mechanical property by forming an extra amount of C-S-H and its hygroscopic porosity, which may provide evaporative cooling on the pavement surface [14,15,35].

2.2.5 Hydrated Lime

Hydrated lime ($Ca(OH)_2$, ≥95% pure) according to IS 712:1984 [36] has been used as an alternate cementitious modifier as shown in **Fig. 1**. Lime was sieved through a 90 μm sieve before use to achieve a uniform fine texture and had a specific gravity of 2.24. Lime has been added as a comparative cementitious modifier because it is known to promote the pozzolanic reactions driven by portlandite and enhance the ITZ densification in the presence of reactive siliceous fines [17].

2.2.6 Recycled Plastic Aggregate (RPA)

The recycled PET-based plastic aggregate used in this study has been obtained from commercial plastics recycling company and was processed by shredding, washing, and grading to obtain the particle size range 10–20 mm which was similar to the coarse aggregate gradation as shown in **Fig. 1**. The RPA's physical properties are as follows: Specific Gravity (1.37); Water Absorption (0.1%), which was practically non-absorbent; and a smooth surface with a hydrophobic character. The thermal conductivity of PET plastic varies between 0·15 and 0·24 W/m·K which is around 6–10 times lower than the thermal

conductivity of granite aggregate (1·5–2·5 W/m·K), meaning RPA is a thermally significant material for UHI mitigation. However, when used in higher amounts, RPA's mechanical stiffness is low and bonding properties are weak, which has to be counterbalanced [21,23,24].

2.2.7 Steel Slag

Steel slag from the steel factory has been collected to use as EAF waste, and left outdoors for aging for at least 6 months in order to decrease the free lime (f-CaO) and periclase (MgO) content, which helps to minimize the volumetric expansion potential. Slag was crushed and sieved to the size similar to Zone II fine aggregate. The processed steel slag had a specific gravity of 3.45 (30% greater than the natural sand), water absorption of 1.8% (high value compared to the Los Angeles abrasion value of the natural coarse aggregate of 16%). Chemical composition by XRF comprised CaO (38.2%), SiO_2 (15.6%), Fe_2O_3 (28.4%), Al_2O_3 (7.2%), MgO (5.8%), MnO (2.1%), and free CaO (1.2% after ageing). Additionally, the high hardness and angularity of steel slag particles provide better aggregate interlocking which also increases the ITZ bond strength, and with a lighter colour than dark coloured natural sand. This additional attribute also contributes to an improvement in surface albedo [18-20].

2.2.8 Superplasticiser and Water

All mixes used a fixed amount of 5 kg/m³ of a polycarboxylate ether-based superplasticiser (SP), in accordance with IS 9103:1999 [37], to keep workability in the slump specified by the target. The water used for mixing and curing is potable water as per IS 456:2000 [38] at a fixed quantity as 160 kg/m³.

2.3 Mix Proportioning

A control mix (C-0) was considered for design based on IS 10262:2019 [39] for M40 grade cement concrete with 28-day characteristic compressive strength of 40 MPa, water-to-binder ratio (w/b) of 0.40, and total binder content of 400 kg/m³. The total content of fine aggregate was set as 650 kg/m³ and coarse aggregate was set as 1200 kg/m³ in all the mixes. The material replacements were carried out so that all observed variations in properties were due to the substitution of materials and not any other factor, and a weight-for-weight basis was used on these within each constituent group. A summary of representative mix proportions for optimum selected mixes at each stage are shown in Table 1.

Table 1. Representative mix proportions for various concrete mixes (kg/m³)

Stage	Mix ID	Cement	Zeolite	Lime	Sand	Steel Slag	Coarse Agg.	RPA	Water	SP
I	C-0	400	0	0	650	0	1200	0	160	5
I	Z-15	340	60	0	650	0	1200	0	160	5
I	L-10	360	0	40	650	0	1200	0	160	5
I	SS-20	400	0	0	520	130	1200	0	160	5
I	RPA-10	400	0	0	650	0	1080	120	160	5
II	Z15R5	340	60	0	650	0	1140	60	160	5
II	Z15R10	340	60	0	650	0	1080	120	160	5
II	L10R5	360	0	40	650	0	1140	60	160	5
II	L10R10	360	0	40	650	0	1080	120	160	5
III	Z15R5S20	340	60	0	520	130	1140	60	160	5
III	Z15R10S20	340	60	0	520	130	1080	120	160	5
III	L10R5S20	360	0	40	520	130	1140	60	160	5
III	L10R10S20	360	0	40	520	130	1080	120	160	5

SP = superplasticiser (polycarboxylate ether, 1.25% by weight of binder). w/b = 0.40. Total binder = 400 kg/m³; total fine aggregate = 650 kg/m³; total coarse aggregate = 1200 kg/m³ for all mixes.

2.4 Specimen Preparation and Curing

For concrete making, the standard procedure was followed using a laboratory pan mixer (100 L capacity). The next steps included; dry mixing of binder constituents (cement + zeolite/lime) for 60 s; addition of the fine aggregate (sand + steel slag) with dry mixing for 60 s; addition of coarse aggregate (granite + RPA) with dry mixing for 60 s; and water was added

incrementally over about 120 s while mixing with superplasticiser pre-mixed in water. Plastic aggregates were added to the mixes containing RPA to ensure uniform distribution. For each batch, fresh concrete was checked and its slump (IS 1199:1959) was found to be in the range 75 – 100 mm.

Specimens were cast in steel moulds coated with oil to form 150 mm cubes for measuring compressive strength, 150 mm diameter × 300 mm height cylinders for split tensile strength, 100 × 100 × 500 mm beams for flexural strength and 300 × 300 × 50 mm slabs for surface temperature measurement. All specimens were compacted on a vibrating table (40 s), covered with polyethylene sheeting, cured for 24 h @ 27 ± 2 °C, demoulded, and placed in curing tanks (water 27 ± 2 °C) until testing.

2.5 Mechanical Testing

Compressive strength was determined by 2000 kN compression testing machine under a compression rate of 14 MPa/min at the ages 7, 28, 56, 90 and 180 days, following IS 516:1959 [40] and split tensile strength was evaluated at the same ages following IS 5816:1999 [41]. The flexural strength under two-point loading (third-point configuration with an effective span of 400 mm) was determined in accordance with IS 516:1959. Three replicate specimens were tested per age per mix; results are reported as mean values are reported. The coefficient of Variation (CoV) was calculated for the consistency of the measurements. The CoV for compressive strength, split tensile strength, and flexural strength ranged between 3.2–4.5%, 4.8–6.5%, and 3.8–5.5%, respectively, all the values are below 6%, which is consistent with the requirements for well-controlled laboratory concrete testing, as given by ACI 214R-11 [42].

2.6 Surface Temperature Measurement

Slab specimens of size (300 × 300 × 50) mm have been used to evaluate surface temperature of each of the 16 Stage III mixes and the control after 28 days curing. As The slabs were placed outdoors on an exposed test bed under clear sky and natural solar radiation showcasing actual field conditions, especially in summer seasons, in Punjab, India (**Fig. 2**). To ensure thermal equilibrium, surface temperatures were taken between 11:00 AM to 4:00 PM at regular intervals of 60 minutes, with a minimum variation of < 0.3 °C between successive readings for 5 minutes, and checked with a calibrated non-contact infrared (IR) thermometer (emissivity of 0.94, spot diameter at 300 mm distance, accuracy ±0.5 °C). The mentioned time frame has been selected due to its ability to contribute to maximum thermal loading and UHI, as verified through literature as well. Five measurement points per specimen (4 corners at 50 mm inset and centre) were set and the arithmetic average of three replicate slabs per mix was reported.

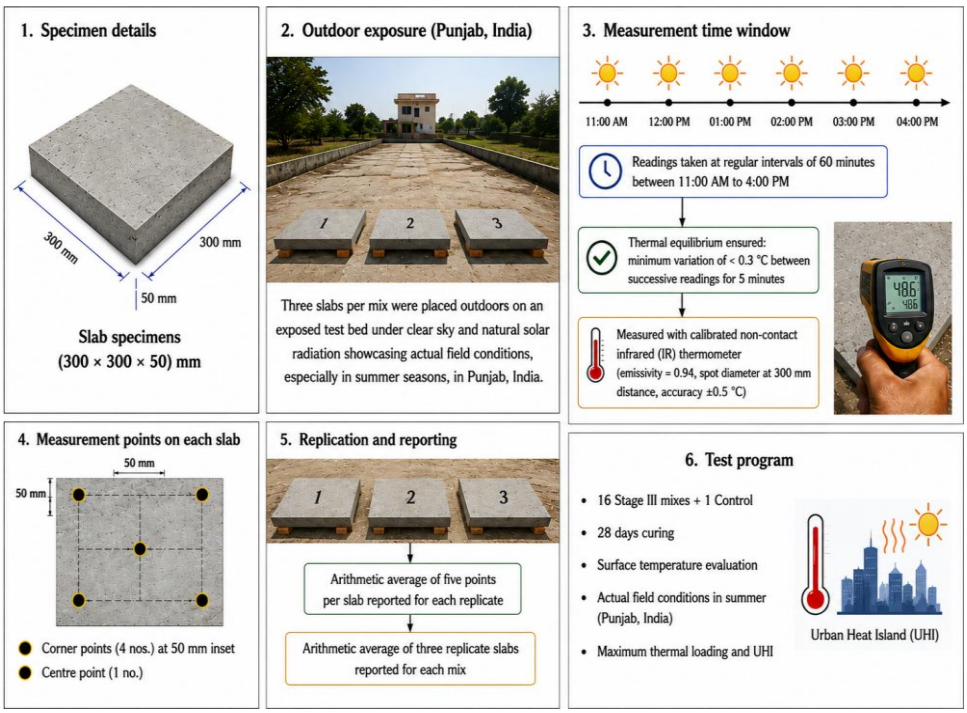


Fig. 2. Experimental Programme for Thermal Analysis

2.7 Statistical Analysis

As the replacement series involved ordered dosage levels, the Jonckheere–Terpstra (J-T) test for ordered alternatives was used to assess ordered trends in the 28-day compressive strength of each Stage I and II material across replacement levels for each material [34]. The J-T test is a non-parametric test which is specifically designed for dose–response data having the hypothesis of a priori ordered trend across k groups, making no distributional assumptions and valid for n = 1 per group applied to group means. For an inverted-U response (zeolite, lime, steel slag), the test was applied to the ascending limb of the curve (control to optimum replacement level) and the descending limb (optimum to 35%) which are two separate directional hypotheses. For RPA, which showed monotonic decreasing patterns at every level, one test was used for all eight ordered groups (0–35%). Computation of one-tailed p-values by a complete enumeration of the k! permutations of the group means was performed. In Stage III, Pearson's product-moment correlation coefficient (r) was calculated for the correlation between 28-day compressive strength and the surface temperature. All computations used Python (SciPy v1.11) at $\alpha = 0.05$.

2.8 Taguchi Design of Experiments for Optimisation Validation

The Taguchi design-of-experiments (DOE) methodology has been used to analyse the dataset for stage III in order to validate the optimum mix identified by the experiments and to quantify the relative contribution of each test variable [30-31]. The 16 mixes in Stage III each represent a specific combination of three controllable factors: Factor A (type of cementitious modifier; two levels); Factor B (RPA content; two levels); Factor C (steel slag content; four levels), for a complete 2×2×4 factorial experiment (Table 2).

Table 2. Taguchi factor assignment for Stage III analysis

Factor	Symbol	Level 1	Level 2	Level 3	Level 4
Cementitious modifier	A	Zeolite 15%	Lime 10%	—	—
RPA content (coarse agg.)	B	5%	10%	—	—
Steel slag content (fine agg.)	C	10%	15%	20%	25%

Factors A and B at 2 levels; Factor C at 4 levels. Full factorial: 2 × 2 × 4 = 16 experimental runs.

For two response variables; (i) the 28-day compressive strength with "larger-is-better" criterion ($S/N = -10 \cdot \log_{10}(1/n \cdot \Sigma 1/y^2_i)$) and (ii) surface temperature with "smaller-is-better" criterion ($S/N = -10 \cdot \log_{10}(1/n \cdot \Sigma y^2_i)$) were computed. With each factor level, Mean S/N ratios were computed to determine the best level of each factor. Testing was carried out by ANOVA on S/N ratios to find the percentage contribution of each factor. The Taguchi analysis was used as an optimisation and factor decomposition method to determine the best combination of the factor levels and estimate the percentage contribution each factor was responsible for the variation in the response. The adequacy of the model (reliability of the additive model as a prediction capable of capturing the system behaviour) was checked by the comparison between the additive model prediction at the identified optimum and the experimentally observed value, alongside the evaluation of possible interaction effects. The inclusion of one of the runs $A_1B_1C_3$ was known as the optimal combination, so the comparison is regarded not as an outside control, but rather as a model adequacy test. In order to confirm generalisability of the additive model, a fully independent validation batch would be required which is currently beyond the present dataset.

3. RESULTS AND DISCUSSION

3.1 Mechanical Performance

3.1.1 Consolidated Comparison of Mechanical Strength across all Stages

The compressive, split tensile and flexural strengths obtained at 28 days for the optimum representative mixes from all the three stages are summarized in a single cross-stage table (Table 3). The overall mechanical performance is outlined in this master comparison, and it serves as a point of reference for the property-specific discussion in the subsequent sections.

Table 3. Consolidated comparison of all three 28-day strength properties across Stages

Stage	Mix	Type	Comp. Str. 28d (MPa)	Split Tensile 28d (MPa)	Flexural Str. 28d (MPa)
Control	C-0	Baseline	44.0	3.80	6.1
I	Z-15	OPC→Zeolite	48.8	4.20	6.8
I	L-10	OPC→Lime	46.0	3.95	6.4
I	SS-20	Sand→Slag	49.5	4.20	6.8
I	RPA-5	CA→RPA	42.0	3.60	6.0
I	RPA-35	CA→RPA	30.5	2.50	4.6
II	Z15R5	Zeo+RPA	48.0	4.20	6.7
II	Z15R20	Zeo+RPA	44.0	3.80	6.1
II	L10R5	Lime+RPA	45.0	3.90	6.3
II	L10R10	Lime+RPA	44.0	3.80	6.1
III	Z15R5S20	Triple optimum	50.5	4.40	7.1
III	L10R5S20	Triple (Lime)	48.5	4.25	6.8
III	L10R10S10	Triple (min.)	45.0	3.90	6.3

All mean values, n = 3 specimens. IRC 58:2015 minimum flexural strength = 4.5 MPa.

Several cross-cutting observations can be made from Table 3. First, a clear performance hierarchy exists among Stage I materials: steel slag (SS-20, +12.5% compressive strength) > zeolite (Z-15, +10.9%) > lime (L-10, +4.5%) > RPA-5 (−4.5%). Secondly, it can be seen that the zeolite has a compensatory effect in Stage II. Z15R5 is able to achieve a 9.1% increase in compressive strength, and L10R5 is able to achieve only 2.3%, while, L10R10 returns to the control level. Third, the triple-replacement Stage III optimum (Z15R5S20) outperforms all the single and double replacements across all the three properties equally (+14.8%, +15.8%, +16.4% for compressive strength, tensile strength and flexural strength, respectively). Lastly, overall, the three strength properties of the data sets trend in the same direction for each mix, but they differ in their magnitudes, providing insight into material specific mechanisms.

3.1.2 Stage I: Effect of Individual Materials on Mechanical Properties

The first stage investigated all the four materials at seven different replacement rates (5–35%). The comprehensive data for compressive, split tensile and flexural strength values at different curing ages are given in **Fig. 3, 4 and 5**. All the three properties exhibited similar behaviour for each material, with few differences observed between them, under certain conditions, that can be described in a mechanistic manner.

Regarding zeolite, a 15% OPC replacement (Z-15) gave the best result for all three properties: the compressive strength was 48.8 MPa (+10.9%), split tensile strength was 4.2 MPa (+10.5%), and flexural strength was 6.8 MPa (+11.5%). The results demonstrated a near proportional enhancement in every loading mode which corresponds to the pozzolanic mechanism of zeolite, adding additional C-S-H that creates uniform densification of the paste and ITZ with all loading directions [11,12]. The split tensile to compressive strength (t/c) and flexural to compressive strength (f/c) ratios (0.086 and 0.139 respectively) were unchanged from the control, confirming proportional scaling. Beyond 15% clinker dilution, it is observed that the pozzolanic contribution is not enough to compensate for the influence of the decreased clinker content. Compressive, split tensile and Flexural strength decreased with increase in clinker proportion with Z-35 showing 37.5 MPa, 3.2 MPa, and 5.3 MPa respectively. At 180 days, Z-15 achieved a compressive strength of 58.6 MPa, whereas the control was 52.8 MPa (+11.0%), which continued to demonstrate pozzolanic C-S-H formation through unreacted clinoptilolite particles, a long-term benefit that is especially relevant to pavements requiring service lives of 30-50 years.

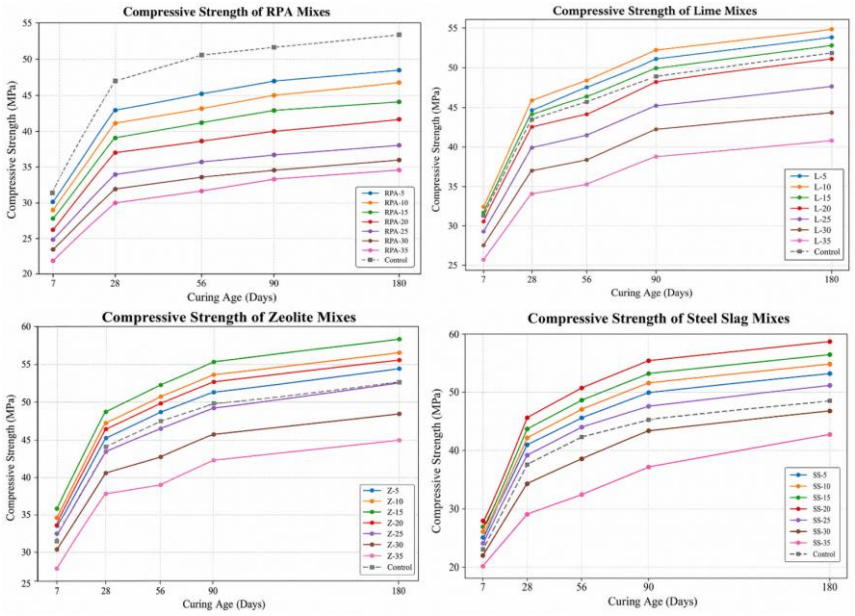


Fig. 3. Compressive strength: Effect of Stage I mixes on supplementary materials.

On replacing OPC with hydrated lime, it was observed that L-10 had modest gains, of similar magnitude, along the three properties i.e. compressive 46.0 MPa (+4.5%), split tensile 3.95 MPa (+3.9%), flexural 6.4 MPa (+4.9%), as shown in (**Fig. 3, 4 and 5)**. Compared to zeolite, lime only contributes to the supplementary portlandite crystallisation and not to the independent formation of C-S-H, limiting the extent and the range of enhancement [17]. As a result, the descending limb was steep, with a flexural strength value of 4.6 MPa for L-35, just barely surpassing the 4.5 MPa rigid pavement requirement specified by IRC 58:2015 [43], thereby, emphasizing the structural risk when high lime doses are used. Most importantly, the percentage increase of L-10 over the control was not different after 28 days (7.9%) or 180 days (4.5%), and this presented a slight disadvantage over zeolite for long-service-life pavement applications.

In case of substitution by Steel slag, SS-20 produced the highest single-material enhancement in Stage I, with, compressive strength as 49.5 MPa (+12.5%), split tensile as 4.2 MPa (+10.5%), and flexural as 6.8 MPa (+11.5%) (**Fig. 3, 4 and 5**). The former (compressive strength) gain is slightly higher because of the cohesive gain in between the slag particles themselves, which is most critical under compression, and a gain on the interface between the slag and the paste, governed by latent hydraulic cementation, more critical under tension. Bending causes the crack tortuosity that is created around the slag particles to stop cracks from growing, and gives the flexural gain in proportion to the compressive gain, not the tensile gain [18]. It can be said that all three properties decrease with increasing residual free CaO and MgO content beyond 20%.

As far as RPA is concerned, at all replacement levels, RPA led to monotonic reduction in all three properties. The decrease, however, did not occur equally: the compressive strength decreased by 4.5%, the tensile strength by 5.3% and the flexural strength by just 1.6%, when the RPA substitution was 5%. This difference, which remains at all levels (35% RPA: −30.7%−34.2%−24.6% respectively), is caused by three factors at the same time: low PET elastic modulus (~2–3 GPa), bond near ITZ hydrophobic which causes ITZ=0, and differential thermal expansion inducing pre-crack effect during curing [21-24]. The quality of the ITZ has a greatest effect on tensile failure as the fracture passes directly through the ITZ whilst, flexural strength is most preserved, as only degradation of the tensile zone of the beam causes the bond failure, with a mechanical averaging effect. This flexural resilience can be quantified by the f/c ratio of RPA-5 (0.143) which is higher than control (0.139). Despite the consistent decrease in strength, RPA's low thermal conductivity (0.15–0.24 W/m·K) warrants its sensible addition at controlled concentrations, on the condition that performance increases are balanced in Stages II and III.

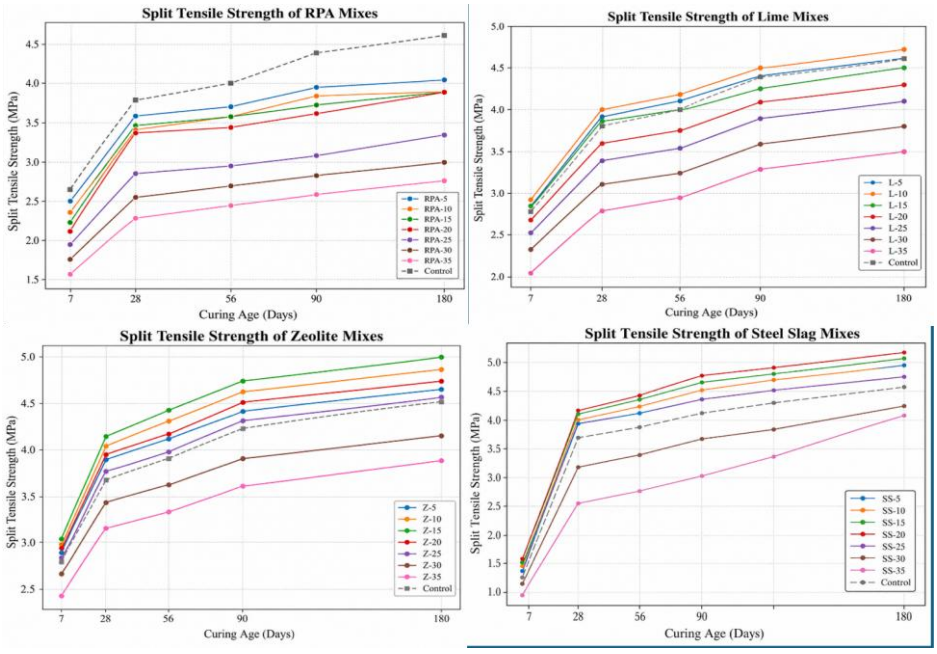


Fig. 4. Split Tensile: Effect of Stage I mixes on supplementary materials.

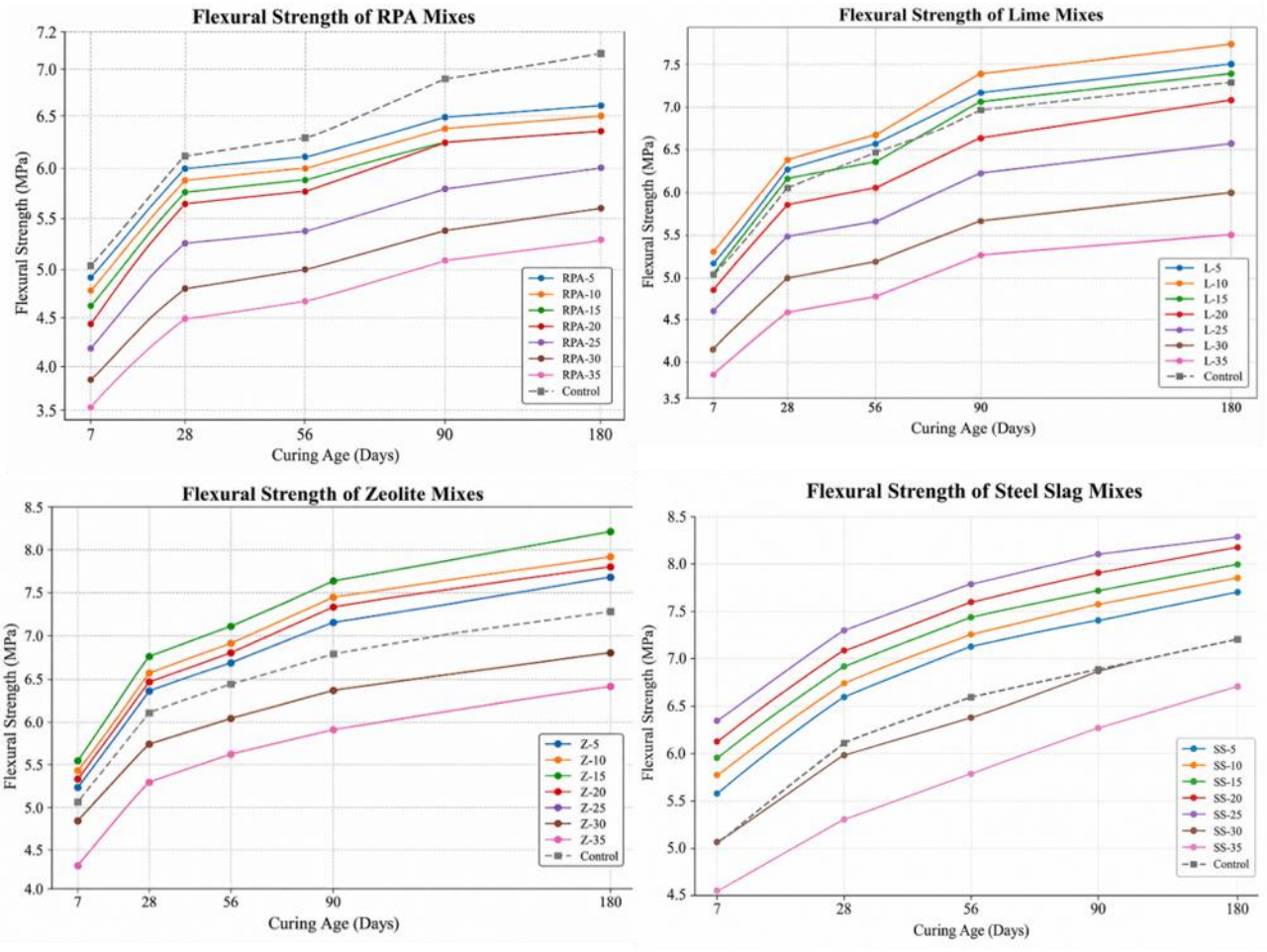


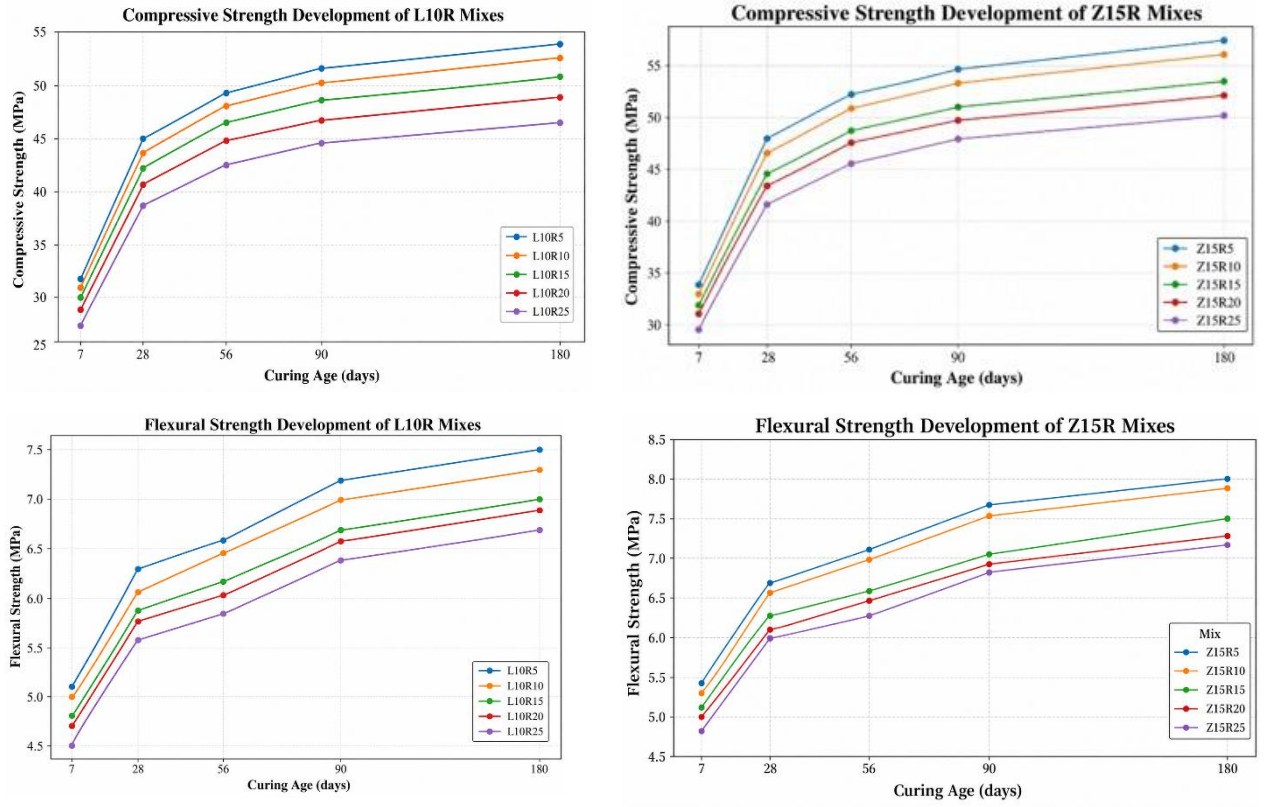
Fig. 5. Flexural Strength: Effect of Stage I mixes on supplementary materials.

3.1.3 Stage II: Compensatory Performance in Double-Replacement Systems

The optimum SCM levels derived in stage-1 were utilized for the design of stage-2 mixes, where, the amount of zeolite was fixed at 15% and lime at 10% cement replacement. Different RPA values (5–25%) were used to investigate, whether the loss of strength due to plastic aggregates could be compensated for by SCM modified matrices. Replacement levels greater than 25% were not considered because of mechanical performance failure in stage 1. Using this approach, controlled assessment of interaction between SCM and RPA was achieved.

The results are shown in **Fig. 6**. Considering Zeolite–RPA series, Z15R5 demonstrated higher compressive strength of 48.0 MPa (+9.1%), tensile strength of 4.2 MPa (+10.5%), and flexural strength of 6.7 MPa (+9.8%) compared with the control, even with 5% RPA content. This verifies the compensatory mechanism of zeolite i.e. the formation of pozzolanic C-S-H matrix can compensate the enlarged porosity of ITZ surrounded by RPA particles and help to increase the ITZ quality to maintain or even improve the macroscopic strength of the paste. Up to 20% RPA (Z15R20: 44.0 MPa (compressive strength), 3.8 MPa (split tensile strength), 6.1 MPa (flexural strength)), the system continued to perform above control, expanding the viable RPA range by three times as compared to individual RPA replacement. However, at >20% RPA, the quantity of poor quality ITZ outweighed zeolite's ability to compensate for the declining properties, and the properties were collectively below the control.

For Lime-RPA series, L10R5 showed +2.3%, +2.6% and +3.3% increase in all the three properties respective to control, whereas L10R10 showed a uniform increase of 1% in all properties. Only the two mixes had mechanical performance equal to or better than the control level, with all three being below 10% RPA. The narrow compensating window (+4.5% Compressive strength) for lime is directly attributable to its smaller pozzolanic output which reduces the surplus strength to balance the deficit created by the RPA. In summary, zeolite–RPA mixes were superior to lime–RPA in tensile and flexural strength, and, at equivalent RPA levels, the compressive strength was 2.0–3.0 MPa higher, agreeing with zeolite being the better cementitious modifier for RPA containing systems.



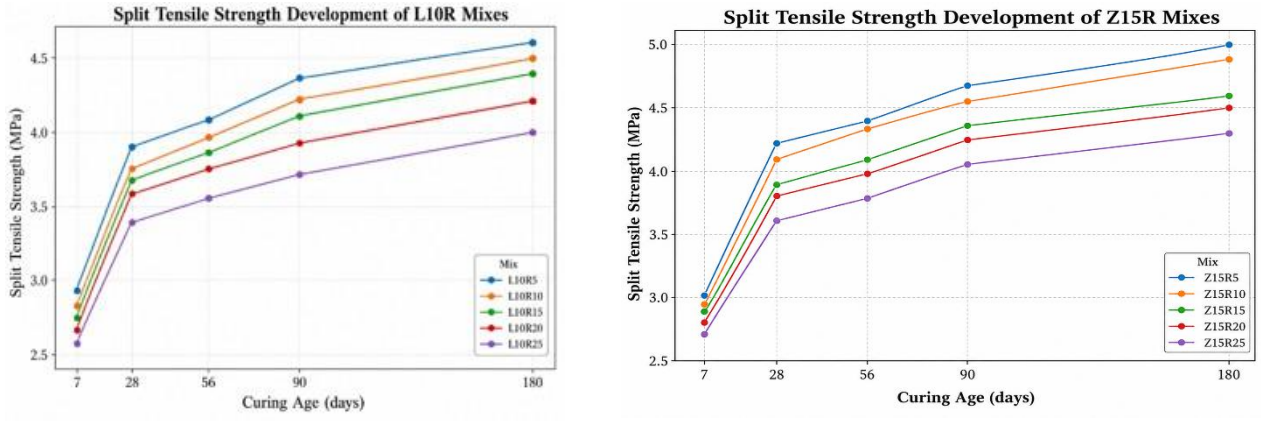


Fig. 6. Effect of Stage II mixes on mechanical properties

3.1.4 Stage III: Mechanical Performance of Triple-Replacement Mixes

In stage III, a total of 16 mixes produced by mixing different proportions of the four optimum modifications (Z15R5, Z15R10, L10R5 and L10R10) derived from stage II, along with the 10–25% replacement of fine aggregate with the steel slag. The mechanical performance of these mixes is summarised in **Fig. 7**. The proportions of steel slag were adjusted from 10–25% and evaluated for the strength, voids and heat dissipation properties. Although 20% showed optimum mechanical performance in Stage 1, 25% was included to examine higher waste utilization and reflective pavement suitability. The results showed that the incorporation of steel slag further provided a quantifiable enhancement of the three strength parameters for all combinations.

Among the zeolite-based series, Z15R5S20 obtained the maximum value of the compressive, split tensile, and flexural strength for the entire 55-mix data set, namely, 50.5 MPa (+14.8%), 4.4 MPa (+15.8%), and 7.1 MPa (+16.4%). The consistency of increment achieved compared to the best double-replacement mix i.e. Z15R5 with compressive strength as 48.0 MPa, split tensile strength as 4.2 MPa, and flexural strength as 6.7 MPa, also validates that steel slag operates on a different microstructural scale to zeolite, namely strengthening the meso-scale aggregate skeleton, derived from angular interlock and crack tortuosity. The two mechanisms are complementary, non-competitive and the combination effect is greater than the individual effect of either material. It can be summarized that the property enhancements of the zeolite/slag mixture on tensile strength (+15.8%) and flexural strength (+16.4%) are greater than on compression (+14.8%), suggesting that the zeolite/slag property enhancements are more pronounced in the compression modes typically relevant to pavement performance.

The 3-property performance for all slag levels remained consistent across all cementitious-RPA combinations and the 20% slag consistently provided the best results; the 10% slag level provided the lowest improvements, and the 25% slag level showed slight deterioration for all the three properties, which may be attributed to the presence of the non-mineralized free CaO, resulting in early onset of volumetric deterioration at higher dosage. With RPA increasing from 5% to 10% in the same cementitious-slag system (e.g., Z15R10S20 versus Z15R5S20), all three properties observed a decrease of ~1.0-2.0 MPa in compressive strength, 0.05–0.15 MPa in split tensile strength, and 0.1–0.2 MPa in flexural strength, which revealed that the triple system remains sensitive to RPA dosage, despite the compensatory effect of zeolite and slag.

The direction was the same but absolute percentage scores were lower for the three mixes using lime. L10R5S20 was found to have compressive, tensile, and flexural strengths of 48.5 MPa (+10.2%), 4.25 MPa (+11.8%), and 6.8 MPa (+11.5%) respectively, which are ~2 MPa lower in compressive strength than its zeolite counterpart due to the differential among the cementitious modifiers established during the Stages I and II tests. All 16 mixes meet the IRC 58:2015 flexural requirement; the lowest flexural for all six Stage III mixes was L10R10S10 (6.3 MPa) which is 40% higher than the minimum value of 4.5 MPa. This full compliance throughout the design space testifies the multi-material approach is structurally flexible to select materials while complying with regulatory requirements.

The triple-material combination maintained its strength benefit at 60.6 MPa at 180 days (+14.8% from the control at 52.8 MPa) with the presence of unreacted zeolite particles to continue with their pozzolanic contribution at late curing ages. The ratio of strength levels for Z15R5S20 (t/c = 0.087, f/c = 0.141) are practically the same as control (0.086 and 0.139), indicating that the three material property changes are consistent in the triple material modification and that there is no loading mode

imbalance in the modified mix. In all three stages and across all three strength properties, Z15R5S20 produces the highest results for every single mix in the 55-mix dataset, with split tensile (+15.8%) and flexural (+16.4%) gains both being superior to the compressive strength increase (+14.8%), thereby, confirming the beneficial effects of this mix formulation in the pavement-relevant loading modes, and declaring it as the clear mechanical optimum status of the entire experimental programme.

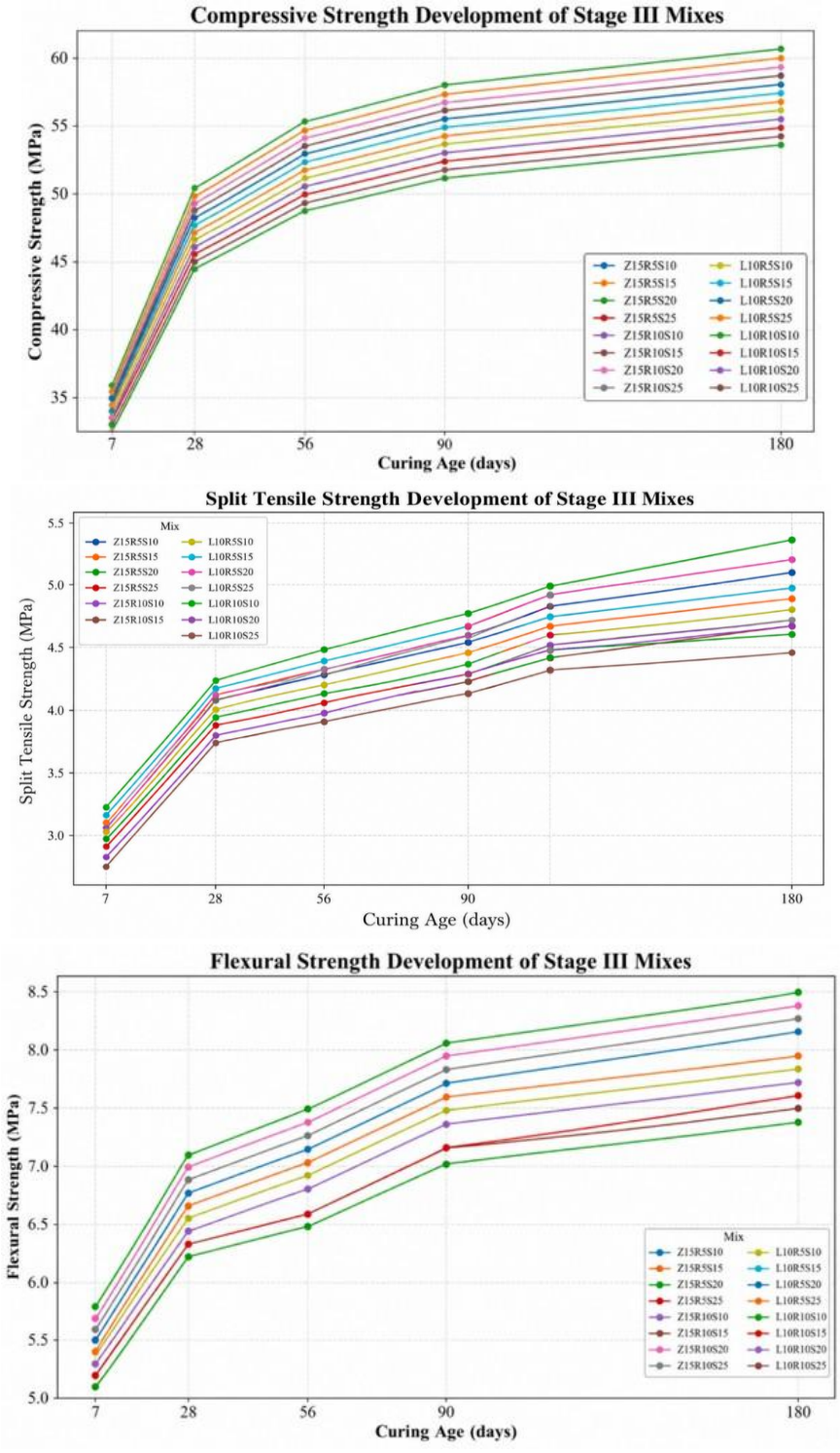


Fig. 7. Effect of Stage III mixes on mechanical properties

3.2 Thermal Performance Analysis

3.2.1 Diurnal Surface Temperature Profiles

The full surface temperature profiles (11:00 to 16:00 h) for all 16 triple-replacement mixes and for the control during natural solar exposure is shown in **Fig. 8**. Regarding the thermal performance analysis, two basic observations are made. For both the control and modified mixes, there was a consistent diurnal trend, with the rise of both mixes starting at 11:00 h followed by a maximum at 14:00 h which was in-phase with peak solar irradiance (900–950 W/m²) and a symmetric decline around 16:00 h. However, temperature rises in all mixes were virtually the same (about 4°C/h between 11:00 and 12:00 h, 3°C/h between 12:00 and 13:00 h, and 1°C/h between 13:00 and 14:00 h), indicating that the changes in the texture of the supplementary material affect the amount of heat absorbed at the surface rather than the rate of response of surface temperature to the solar heat input. This is in line with the materials' mode of operation, which is believed to be largely surface albedo modification and thermal emissivity changes, rather than changing bulk thermal mass [38,39]. Secondly, and more importantly, the thermal benefit of every mix modified was determined from the first recording at 11:00 h which remained constant over the monitoring period for the purpose of UHI assessment. Z15R5S20 recorded 43.0 °C at 11:00 h versus 50.0 °C for the control (−7.0°C), and 50.5°C at the 14:00 h peak versus 58.0 °C (−7.5 °C), as shown in table 4. The change from a narrow to a wide differential margin during the morning and peak suggests that the thermal separation is not a temporal artifact of measurements, but a reduction in heat storage on the surface averaged over time during the solar day.

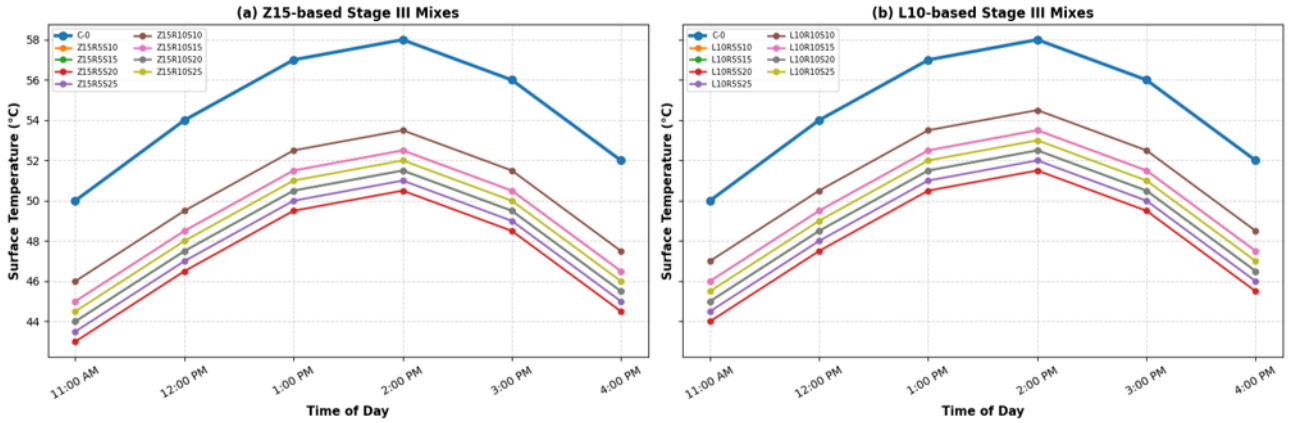


Fig. 8. Diurnal surface temperature variation of Stage III and control mixes under natural solar exposure.

Note: All values in °C. Surface temperature measured by IR thermometer (emissivity 0.94; accuracy ±0.5°C)

Table 4. Comparison of morning (11:00 h) and peak (14:00 h) surface temperature reductions for representative mixes

Mix ID	Series	11:00 h (°C)	14:00 h Peak (°C)	Peak Red. (°C)	Reduc. at 11:00 h (°C)
C-0	Control	50.0	58.0	—	—
Z15R5S20	Z15 + RPA5	43.0	50.5	−7.5	−7.0
Z15R5S10	Z15 + RPA5	45.0	52.5	−5.5	−5.0
Z15R10S20	Z15 + RPA10	44.0	51.5	−6.5	−6.0
L10R5S20	L10 + RPA5	44.0	51.5	−6.5	−6.0
L10R5S10	L10 + RPA5	46.0	53.5	−4.5	−4.0
L10R10S20	L10 + RPA10	45.0	52.5	−5.5	−5.0
L10R10S10	L10 + RPA10	47.0	54.5	−3.5	−3.0

Reduction = T(C-0) − T(mix) at respective time. Consistent reduction from 11:00 h to peak confirms sustained thermal benefit throughout the solar day.

3.2.2 Factors Governing Thermal Behaviour

The systematic difference among the surface temperatures for the 16 mixes shows the contributions of three mechanisms that depend on the material properties. Within each of the cementitious–RPA series, a 10% to 20% increase in steel slag content produced a consistent 2.0 °C drop in peak temperature for each series (e.g. Z15R5S10, 52.5°C; Z15R5S20, 50.5°C), whereas, an increase from 20% to 25% in steel slag, had a marginal decrease of 0.5 °C. It was concluded, based on consistently lower temperatures for higher slag contents across all measurement hours, that the particles of the EAF slag reflect a higher proportion of incident solar radiation during the day compared with the particles of natural sand, stemming from the lighter colour and higher albedo of the slag particles [14,15,42].

Higher RPA content (10% versus 5%) consistently recorded 1.0°C increase in peak temperature for the same slag and cementitious environments. The lower bulk thermal conductivity of RPA does not hinder its ability to trap the solar heat within the near surface micro-voiding of the RPA-paste ITZ and maintain high surface temperatures as indicated by the earlier measurements at 11:00 h and as late as 16:00 h [18,43]. Corresponding lime- and zeolite-based mixes showed that the zeolite-based mixes experienced peak temperatures around 1.0°C lower, at the same RPA and slag contents, which is in accordance with the hygroscopic porosity of zeolite allowing evaporative cooling during the duration of the test [45]. The comparison of all zeolite-based versus lime-based peak temperatures with a two-sample t-test gave $t = -2.10$, $p = 0.055$. The results indicate that there is a marginal yet significant difference in the temperature variations among the zeolite and lime-based mixes.

3.2.3 Mechanical–Thermal Relationship and Concurrent Optimality

The strong negative Pearson correlation ($r = -0.83$, $p < 0.001$, $R^2 = 0.69$), found between 28-day compressive strength and peak surface temperature for all 16 Stage III mixes (**Fig. 9**), confirms that the mechanical enhancement process and the thermal mitigating process are complementary and do not counterbalance each other in this material system. The mix that yielded the largest enhancement in mechanical properties for all three types (Z15R5S20) also resulted in the highest reduction in temperature during the monitoring, with a peak temperature reduction by 7.5°C and the reduction at 11:00 has 7.0°C, thus demonstrating the concurrent 4-dimensional optimality. This outcome contradicts the implicit assumption in cool pavement literature that there is a compromise between thermal and structural goals [3,7-11].

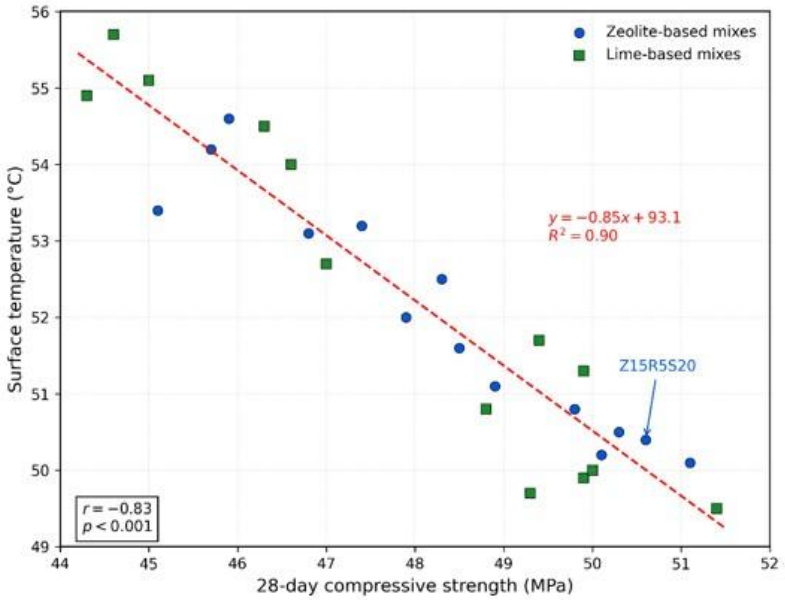


Fig. 9. Pearson correlation between 28-day compressive strength and peak (14:00 h) surface temperature for all Stage III mixes.

3.3 Statistical Validation

3.3.1 Jonckheere–Terpstra Test: Significance of Ordered Trends in Stage I and II

The J-T test of ordered alternatives was used for 28-day group means of the compressive strength of each of the material series in Stage I and II [44]. The test does not rely on any assumptions about distribution and is valid for n = 1 group, directly applicable to the group means reported here. One-tailed p-values were determined by complete enumeration of permutations. The results are shown in table 5 and 6.

For zeolite, both ascending (C-0→Z-15, p = 0.042) and descending (Z-15→Z-35, p = 0.008) limbs exhibited statistically significant ordered trends, thereby enhancing the validity of the inverted-U response model with Z-15 being the optimum condition. In case of lime, the relatively weak increase in strength with increasing replacement (+4.5% at 10% lime replacement) is likely a tendency rather than a statistically significant improvement given the information in the group-level data at hand. The trend is downward from 10%, and is significant at the 0.001 level, verifying the rapid decrease with increased doses. In case of steel slag, both the ascent (C-0 to SS-20; p = 0.008) and decent (SS-20 to SS-35; p = 0.042) limbs are statistically significant with SS-20 as the optimum. For RPA, all eight ordered groups (C-0 to RPA-35) showed a monotonic decreasing trend: J = 28/28, p < 0.001, which validates that RPA causes consistent ordered strength reduction across all replacement levels.

The decreasing tendency for Z15+RPA (J = 21/21, p < 0.001) and L10+RPA (J = 21/21, p < 0.001) is confirmed by the fact that RPA-induced strength reduction is an actual ordered effect in both double-replacement systems (Table 6). A statistically sound basis is provided for the material selection for Stage III, as the zeolite consistently performs better than lime at all seven matched RPA dosages (based on a sign test, 7/7 in favour of zeolite, p = 0.008).

Table 5. J-T test results for ordered trends in 28-day compressive strength across Stage I replacement levels.

Material	Limb	k (groups)	J / J_{max}	p-value (exact, one-tailed)	Conclusion
Zeolite	Ascending (C-0→Z-15)	4	6 / 6	0.042	Significant increasing *
	Descending (Z-15→Z-35)	5	10 / 10	0.008	Significant decreasing *
Lime	Ascending (C-0→L-10)	3	3 / 3	0.167	Non-significant trend
	Descending (L-10→L-35)	6	15 / 15	0.001	Significant decreasing *
Steel slag	Ascending (C-0→SS-20)	5	10 / 10	0.008	Significant increasing *
	Descending (SS-20→SS-35)	4	6 / 6	0.042	Significant decreasing *
RPA	Monotonic descending (all)	8	28 / 28	< 0.001	Significant decreasing *

*J = observed J-T statistic; J_{max} = maximum possible J for k groups. Exact one-tailed p-values by full permutation enumeration. * p < 0.05.*

Table 6. J-T test results for Stage II double-replacement series

Series	Test	k (groups)	J / J_{max}	Conclusion
Z15+RPA	Descending (Z15R5→Z15R35)	7	21 / 21	Significant ***

L10+RPA	Descending (L10R5→L10R35)	7	21 / 21	Significant ***
Z15+RPA vs L10+RPA	Sign test (7 matched pairs)	7	7 / 7	Z15 > L10 at all levels **

*** $p < 0.01$; *** $p < 0.001$.*

3.3.2 Pearson Correlation: Mechanical and Thermal Performance

The Pearson correlation between the 28-day compressive strength and surface temperature for all 16 of the Stage III mixes was reported to be $r = -0.83$ ($p < 0.001$; $R^2 = 0.69$) (Fig. 12). Observed r value substantially exceeds the critical r value (approx ±0.71) for $n = 16$ and $\alpha = 0.001$, indicating statistical robustness. The 31% unexplained variance is attributable to material-specific thermal mechanisms which are correlated but not fully described by compressive strength alone, further supporting the complementary nature of mechanical and thermal properties of this system.

3.4 Taguchi Optimisation and Factor Contribution Analysis

3.4.1 Signal-to-Noise Ratios and Optimum Identification

Table 7 shows the S/N ratios for compressive strength (larger-is-better) and surface temperature (smaller-is-better) for all 16 Stage III mixes, as well as all three of the 28-day strength properties to illustrate full traceability. The data set in Stage III shows that Z15R5S20 ($A_1B_1C_3$) achieves the largest values for both tensile (4.40 MPa) and flexural (7.1 MPa) strength, with the highest S/N being 34.066 dB for compressive strength and the least negative S/N being −34.066 dB for surface temperature. The Taguchi S/N analysis, therefore, confirms the mix obtained from the experimental ranking as the optimum mix.

Table 7. Signal-to-noise ratios and full mechanical data for Stage III mixes (Taguchi analysis)

Mix ID	A	B	C	Comp. 28d	S/N Comp. (dB)	Tens. 28d	Flex. 28d	Surf. Temp.	S/N Temp. (dB)
Z15R5S10	1	1	1	49.0	33.804	4.30	6.9	52.5	−34.402
Z15R5S15	1	1	2	50.0	33.979	4.35	7.0	51.5	−34.235
Z15R5S20	1	1	3	50.5	34.066	4.40	7.1	50.5	−34.066
Z15R5S25	1	1	4	49.5	33.892	4.30	7.0	51.0	−34.152
Z15R10S10	1	2	1	48.0	33.625	4.20	6.8	53.5	−34.566
Z15R10S15	1	2	2	49.0	33.804	4.30	6.9	52.5	−34.402
Z15R10S20	1	2	3	49.5	33.892	4.35	7.0	51.5	−34.235
Z15R10S25	1	2	4	48.5	33.715	4.25	6.9	52.0	−34.319
L10R5S10	2	1	1	47.0	33.442	4.10	6.6	53.5	−34.566
L10R5S15	2	1	2	48.0	33.625	4.20	6.7	52.5	−34.402
L10R5S20	2	1	3	48.5	33.715	4.25	6.8	51.5	−34.235
L10R5S25	2	1	4	47.5	33.534	4.15	6.7	52.0	−34.319
L10R10S10	2	2	1	45.0	33.064	3.90	6.3	54.5	−34.729
L10R10S15	2	2	2	46.0	33.255	4.00	6.4	53.5	−34.566
L10R10S20	2	2	3	46.5	33.349	4.05	6.5	52.5	−34.402
L10R10S25	2	2	4	45.5	33.160	3.95	6.4	53.0	−34.487

S/N Comp. $= -10 \cdot \log_{10}(1/y^2)$; *S/N Temp.* $= -10 \cdot \log_{10}(y^2)$. *A=1: Zeolite 15%, A=2: Lime 10%; B=1: RPA5%, B=2: RPA10%; C=1–4: Slag 10–25%.*

3.4.2 Main Effects and Factor Contribution

Mean S/N ratios by factor level are reported in Table 8. In terms of compressive strength, ranking factors are A > B > C, where cementitious modifier type is the most influencing factor (+0.454 dB delta), followed by RPA content (+0.274 dB) and steel slag (+0.272 dB). In terms of surface temperature, the ranks are reversed to C > A = B, with the steel slag content being the dominant (+0.331 dB), and cementitious type (+0.166 dB) and the RPA content (+0.166 dB) being similarly influential factors. This inversion is consistent with the mechanistic performance observed in Sections 4.1 and 4.2; zeolite dominates control over the mechanical strength in the paste but does not show a significant contribution towards thermal performance, whilst, steel slag shows a dominant contribution for the surface albedo and thermal diffusivity.

The complete ANOVA table for S/N ratio based on all the main effects and interaction is given in Table 9. The total S/N variation for compressive strength and surface temperature are 97.1% and nearly 100% for the main effects, respectively. The only significant interaction is A×B, cementitious type × RPA content, with its value of 2.9% indicating the relatively weak dependence of the cementitious type on RPA content, as seen above, where the pozzolanic output of the zeolite provides a greater dependency on the RPA content than on the type of cementitious material used. The combined effect of all other interactions (A×C, B×C, A×B×C) is less than 0.01% for both responses, which further supports that steel slag has little interaction with either the cementitious modifier or RPA content. The contribution from total interactions, 2.9% (strength) and near zero (≈0% (temperature)) reflects the validity of considering the additive model as a valid approximation to the system behaviour for this material combination, also supported by **fig. 10**.

Table 8. Mean S/N ratios by factor level and sensitivity ranking (Taguchi main effects)

Factor	Level	Description	Mean S/N Comp. (dB)	Mean S/N Temp. (dB)	Delta Comp.	Delta Temp.	Rank Comp.	Rank Temp.
A: Cementitious	1	Zeolite 15%	33.847	−34.298				
	2	Lime 10%	33.393	−34.464	0.454	0.166	1	2
B: RPA content	1	5%	33.757	−34.298				
	2	10%	33.483	−34.464	0.274	0.166	2	2
C: Steel slag	1	10%	33.484	−34.566				
	2	15%	33.666	−34.402				
	3	20%	33.755	−34.235				
	4	25%	33.575	−34.319	0.272	0.331	3	1

Delta = max − min mean S/N within each factor. Rank 1 = most influential.

Table 9. ANOVA on S/N ratios: percentage factor contribution to response variation.

Source	df	SS Comp.	% Cont. Comp.	SS Temp.	% Cont. Temp.
A: Cementitious	1	0.82492	62.1%	0.11039	24.0%
B: RPA content	1	0.30058	22.6%	0.11039	24.0%
C: Steel slag	3	0.16408	12.4%	0.23926	52.0%
A×B	1	0.03832	2.9%	0.00000	0.0%
A×C	3	0.00012	0.0%	0.00001	0.0%
B×C	3	0.00004	0.0%	0.00001	0.0%
A×B×C	3	0.00001	0.0%	0.00000	0.0%
Total	15	1.32806	100%	0.46007	100%

SS = sum of squares of S/N ratios. % Contribution = SS(factor)/SS(total) × 100.

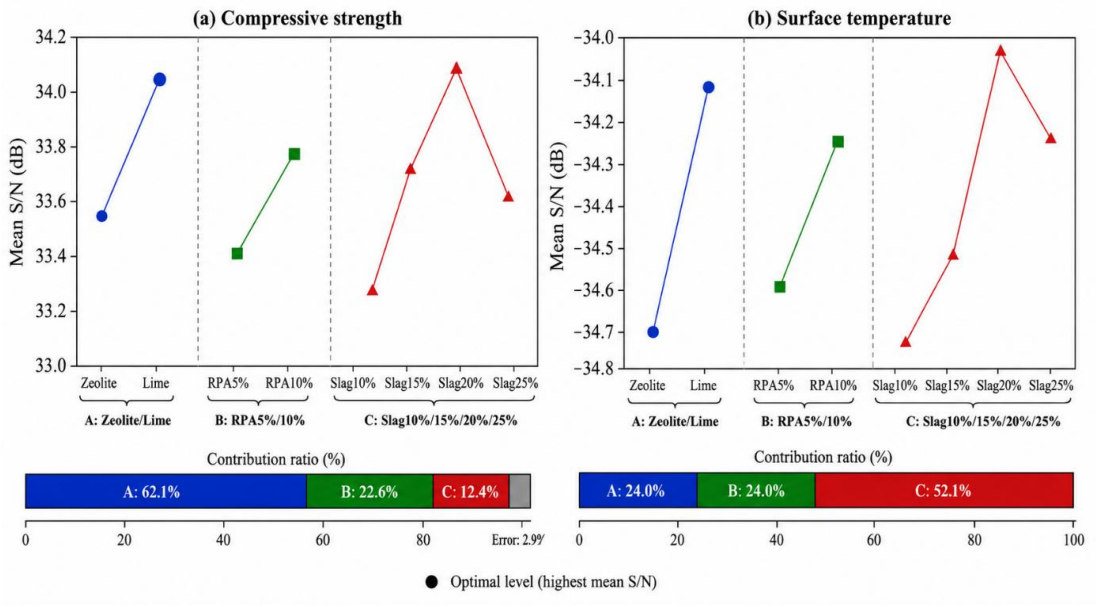


Fig. 10. Taguchi main effects plots: (a) compressive strength and (b) surface temperature, with percentage contribution bar below each panel.

3.4.3 Confirmation Test and Model Validation

The prediction for $A_1B_1C_3$ (1/8 of each of the three relevant marginal means) in the additive model was calculated as: predicted S/N = grand mean + (A_1 marginal mean − grand mean) + (B_1 marginal mean − grand mean) + (C_3 marginal mean − grand mean). Therefore, the prediction is model driven and not a direct reporting of the observed quantity. This agrees with the interaction ANOVA shown in Table 9 which have total interaction SS of only 2.9 % for compressive strength and insignificant for surface temperature and falls within the 10 percent model adequacy criterion of Ross [21] that was established through the errors of prediction. It is recognised that one of the original 16 factorial runs was $A_1B_1C_3$ (Z15R5S20), but was not a fully independent confirmation batch, as is the case with the present Taguchi application. This analysis is thus used as an optimisation tool and a factor decomposition tool, to provide analytical support for the selection of Z15R5S20 as the optimal combination (Table 10).

Table 10. Taguchi confirmation test for optimum mix Z15R5S20 ($A_1B_1C_3$)

Response	Optimal ($A_1B_1C_3$)	Pred. S/N (dB)	Actual S/N (dB)	Predicted	Actual	Error (%)	Valid?
Comp. strength	Zeo 15%+RPA 5%+Slag 20%	34.120	34.066	50.8 MPa	50.5 MPa	0.62	Yes
Surf. temperature	Zeo 15%+RPA 5%+Slag 20%	−34.069	−34.066	50.5 °C	50.5 °C	0.04	Yes

Validity criterion: error < 10% [21]. A_1 = Zeolite 15%; B_1 = RPA 5%; C_3 = Steel slag 20%.

4. CONCLUSIONS

A three-stage experimental program was performed with 55 concrete mix designs to assess the mechanical properties and surface temperature reduction capabilities of rigid pavement concrete containing supplementary cementitious materials (SCMs). Compressive strength, split tensile strength, flexural strength, thermal performance were evaluated, and one-way ANOVA, Pearson correlation, Jonckheere-Terpstra trend analysis and Taguchi Design of Experiments (DOE) were used. The use of natural zeolite partially replaced 15% of OPC in Stage I, which led to an increase of 10.9% in compressive strength, 10.5% in split tensile strength, and 11.5% in flexural strength while 10% hydrated lime showed moderate strength gain. The use of steel slag as a fine aggregate replacement resulted in the highest increment of compressive strength (12.5%), while the mechanical properties of the mixes decreased gradually with the higher proportion of recycled PET aggregate (RPA) used,

with flexural strength being the least affected. The ordered trends of zeolite, steel slag and RPA replacement levels were confirmed by statistical analysis. The strength losses resulting from the addition of RPA are compensated for by the use of 15% zeolite up to 20% RPA, and hydrated lime can only do so to a certain extent. The optimum mix composition (Z15R5S20) used in Stage III produced compressive, split tensile and flexural strengths of 50.5 MPa, 4.4 MPa and 7.1 MPa, respectively, which are above the minimum requirement set by IRC 58:2015 by 14.8%, 15.8% and 57.8%. This optimized combination also decreased the temperature of the pavement surface by 7.5 °C under natural solar radiation, which proved to be a significant potential mitigation for urban heat island (UHI) effects. The compressive strength and the surface temperature showed a strong negative correlation ($r = -0.83$, $p < 0.001$), suggesting that improved structural performance and thermal mitigation can be obtained by the same time. The taguchi signal to noise analysis confirmed Z15R5S20 as dual response optimum mix with minimum number of confirmation errors and factor contribution analysis showed that the value of compressive strength was more influenced by cementitious modifier and the value of thermal performance was more influenced by the value of steel slag content. Optimized mix not only resulted in a mix that used 60 kg of OPC per cubic metre of concrete, but also combined 60 kg of post-consumer PET waste with 130 kg of industrial EAF steel slag, diverting some 190 kg/m³ of waste from landfill while delivering the same structural performance. The results have indicated that the SCM-based concrete can be a viable solution for sustainable climate responsive pavement infrastructure, while adhering to the principles of circular economy. Future studies would include long-term durability, field-scale thermal testing with different environmental loads, heat conductivity testing, and albedo and solar reflectivity measurements, as well as extensive economic and carbon footprint assessments, to address these issues.

Statements & Declarations

There is no conflict of interest among authors.

Funding

This research did not receive any specific grant from funding agencies in the public, commercial, or not-for-profit sectors.

Acknowledgement

The authors are thankful to Chitkara University for providing all the facilities.

REFERENCES

[1] Oke, T.R. (1982). The energetic basis of the urban heat island. Q. J. R. Meteorol. Soc., 108(455), 1–24. https://doi.org/10.1002/qj.49710845502

[2] Santamouris, M. (2013). Using cool pavements as a mitigation strategy to fight urban heat island. Renew. Sustain. Energy Rev., 26, 224–240. https://doi.org/10.1016/j.rser.2013.05.047

[3] Qin, Y. (2015). A review on the development of cool pavements to mitigate urban heat island effect. Renew. Sustain. Energy Rev., 52, 445–459. https://doi.org/10.1016/j.rser.2015.07.177

[4] Santamouris, M. (2020). Recent progress on urban overheating and heat island research. Integrated assessment of the energy, environmental, vulnerability and health impact. Synergies with the global climate change. Energy Build., 207, 109482. https://doi.org/10.1016/j.enbuild.2019.109482

[5] Akbari, H., & Kolokotsa, D. (2016). Three decades of urban heat islands and mitigation technologies research. Energy Build., 133, 834–842. https://doi.org/10.1016/j.enbuild.2016.09.067

[6]] Nwakaire, C.M., Onn, C.C., Yap, S.P., Yuen, C.W., & Onodagu, P.D. (2020). Urban Heat Island studies with emphasis on urban pavements: A review. Sustain. Cities Soc., 63, 102476. https://doi.org/10.1016/j.scs.2020.102476

[7] Mohajerani, A., Bakaric, J., & Jeffrey-Bailey, T. (2017). The urban heat island effect and thermal properties of asphalt concrete. J. Environ. Manage., 197, 522–538. https://doi.org/10.1016/j.jenvman.2017.03.095

[8] Kappou, S., Souliotis, M., Papaefthimiou, S., Panaras, G., Paravantis, J.A., Michalena, E., Hills, J.M., Vouros, A.P., Ntymenou, A., & Mihalakakou, G. (2022). Cool pavements: State of the art and new technologies. Sustainability, 14(9), 5159. https://doi.org/10.3390/su14095159

[9] Santamouris, M., & Yun, G.Y. (2020). Recent development and research priorities on cool and super cool materials to mitigate urban heat island. Renew. Energy, 161, 792–807. https://doi.org/10.1016/j.renene.2020.07.109

[10] Li, H., Harvey, J.T., Holland, T.J., & Kayhanian, M. (2013). Reflective and permeable pavements for heat island mitigation. Environ. Res. Lett., 8(1), 015023. https://doi.org/10.1088/1748-9326/8/1/015023

[11] Ko, J., Schlaerth, H., Bruce, A., Sanders, K., & Ban-Weiss, G. (2022). Measuring the impacts of a real-world neighborhood-scale cool pavement deployment on albedo and temperatures in Los Angeles. Environ. Res. Lett., 17(4), 044027. https://doi.org/10.1088/1748-9326/ac58a8

[12] Andrew, R.M. (2019). Global CO_2 emissions from cement production, 1928–2018. Earth Syst. Sci. Data, 11(4), 1675–1710. https://doi.org/10.5194/essd-11-1675-2019

[13] Ahmadi, B., & Shekarchi, M. (2010). Use of natural zeolite as a supplementary cementitious material. Cem. Concr. Compos., 32(2), 134–141. https://doi.org/10.1016/j.cemconcomp.2009.10.006

[14] Tran, Y.T., Lee, J., Kumar, P., Kim, K.-H., & Lee, S.S. (2019). Natural zeolite and its application in concrete composite production. Compos. Part B Eng., 165, 354–364. https://doi.org/10.1016/j.compositesb.2018.12.084

[15] Shekarchi, M., Ahmadi, B., Azarhomayun, F., Shafei, B., & Kioumarsi, M. (2023). Natural zeolite as a supplementary cementitious material – A holistic review of main properties and applications. Constr. Build. Mater., 409, 133766. https://doi.org/10.1016/j.conbuildmat.2023.133766

[16] Valipour, M., Pargar, F., Shekarchi, M., & Khani, S. (2013). Comparing zeolite to metakaolin and silica fume for durability. Constr. Build. Mater., 41, 879–888. https://doi.org/10.1016/j.conbuildmat.2012.11.054

[17] Arandigoyen, M., & Alvarez, J.I. (2007). Pore structure and mechanical properties of cement-lime mortars. Cem. Concr. Res., 37(5), 767–775. https://doi.org/10.1016/j.cemconres.2007.02.023

[18] Manso, J.M., Polanco, J.A., Losanez, M., & Gonzalez, J.J. (2006). Durability of concrete made with EAF slag. Cem. Concr. Compos., 28(6), 528–534. https://doi.org/10.1016/j.cemconcomp.2006.02.008

[19] Maslehuddin, M., et al. (2003). Comparison of steel slag and crushed limestone aggregate concretes. Constr. Build. Mater., 17(2), 105–112. https://doi.org/10.1016/S0950-0618(02)00095-8

[20] Arribas, I., Santamaría, A., Ruiz, E., Ortega-López, V., & Manso, J.M. (2015). Electric arc furnace slag and its use in hydraulic concrete. Constr. Build. Mater., 90, 68–79. https://doi.org/10.1016/j.conbuildmat.2015.05.003

[21] Gu, L., & Ozbakkaloglu, T. (2016). Use of recycled plastics in concrete: A critical review. Waste Manage., 51, 19–42. https://doi.org/10.1016/j.wasman.2016.03.005

[22] Siddique, R., Khatib, J., & Kaur, I. (2008). Use of recycled plastic in concrete: A review. Waste Manage., 28(10), 1835–1852. https://doi.org/10.1016/j.wasman.2007.09.011

[23] Ismail, Z.Z., & Al-Hashmi, E.A. (2008). Waste plastic as aggregate replacement. Waste Manage., 28(11), 2041–2047. https://doi.org/10.1016/j.wasman.2007.08.023

[24] Qaidi, S., Al-Kamaki, Y., Hakeem, I., Dulaimi, A.F., Özkılıç, Y., Sabri, M., & Sergeev, V. (2023). Investigation of the physical-mechanical properties and durability of high-strength concrete with recycled PET as a partial replacement for fine aggregates. Front. Mater., 10, 1101146. https://doi.org/10.3389/fmats.2023.1101146

[25] Sharma, R., & Bansal, P.P. (2016). Waste plastic in concrete. J. Clean. Prod., 112, 473–482. https://doi.org/10.1016/j.jclepro.2015.08.042

[26] Juenger, M.C., & Siddique, R. (2015). Recent advances in supplementary cementitious materials in concrete. Cem. Concr. Res., 78, 71–80. https://doi.org/10.1016/j.cemconres.2015.03.018

27] Siddique, R., & Klaus, J. (2009). Influence of metakaolin on mortar and concrete properties. Appl. Clay Sci., 43(3–4), 392–400. https://doi.org/10.1016/j.clay.2008.11.007

[28] Delatte, N.J. (2014). Concrete Pavement Design, Construction, and Performance (2nd ed.). CRC Press. (Book — no DOI)

[29] Thomas, B.S., & Gupta, R.C. (2016). Waste tire rubber in cement concrete. Renew. Sustain. Energy Rev., 54, 1323–1333. https://doi.org/10.1016/j.rser.2015.10.092

[30] Ross, P.J. (1996). Taguchi Techniques for Quality Engineering (2nd ed.). McGraw-Hill. (Book — no DOI)

[31] Teimortashlu, E., Dehestani, M., & Jalal, M. (2018). Application of Taguchi method for compressive strength optimization of tertiary blended self-compacting mortar. Constr. Build. Mater., 190, 1182–1191. https://doi.org/10.1016/j.conbuildmat.2018.09.165

[32] Montgomery, D.C. (2017). Design and Analysis of Experiments (9th ed.). John Wiley & Sons. (Book — no DOI)

[33] IS 8112 (2013). OPC, 43 Grade – Specification. Bureau of Indian Standards. (Standard — no DOI)

[34] IS 383 (2016). Coarse and Fine Aggregate for Concrete – Specification. BIS. (Standard — no DOI)

[35] Pancar, E.B. (2016). Using recycled glass and zeolite in concrete pavement to mitigate heat island and reduce thermal cracks. Adv. Mater. Sci. Eng., 2016, 8526354. https://doi.org/10.1155/2016/8526354

[36] IS 712 (1984). Specification for Building Limes. BIS. (Standard — no DOI)

[37] IS 9103 (1999). Specification for Concrete Admixtures. BIS. (Standard — no DOI)

[38] IS 456 (2000). Plain and Reinforced Concrete – Code of Practice. BIS. (Standard — no DOI)

[39] IS 10262 (2019). Concrete Mix Proportioning – Guidelines. BIS. (Standard — no DOI)

[40] IS 516 (1959). Methods of Tests for Strength of Concrete. BIS. (Standard — no DOI)

[41] IS 5816 (1999). Splitting Tensile Strength of Concrete. BIS. (Standard — no DOI)

[42] ACI 214R-11 (2011). Guide to Evaluation of Strength Test Results of Concrete. ACI. (Standard — no DOI)

[43] IRC:58 (2015). Guidelines for Design of Plain Jointed Rigid Pavements. Indian Roads Congress. (Standard — no DOI)

[44] Jonckheere, A.R. (1954). A distribution-free k-sample test against ordered alternatives. Biometrika, 41(1–2), 133–145. JSTOR: https://www.jstor.org/stable/2333011 (Pre-DOI era SCI journal)

[45] ASTM C618 (2023). Standard Specification for Coal Fly Ash and Raw or Calcined Natural Pozzolan. ASTM International. (Standard — no DOI)